Chapter 15
Multi-Scale Mechanical Performance of High Strength-High Ductility Concrete

Ravi Ranade, William F. Heard, and Brett A. Williams

Abstract A new fiber-reinforced cement-based composite, called High Strength-High Ductility Concrete (HSHDC) with unparalleled combination of compressive strength (>150 MPa) and tensile ductility (>3 %), has been recently developed. Due to such unique combination of properties, the specific energies of HSHDC under tension and compression at both pseudo-static and high strain rates are extremely high. The design of this engineered material is based on the fundamental principles of micromechanics which focus on the synchronous functioning of the fiber, the cementitious matrix, and their interface to achieve the desired material properties for a given structural application. For such micromechanics-based design to succeed, the material has been researched at several length scales ranging from micro-scale fiber/matrix interactions to structural-scale impact resistance of HSHDC slabs. This paper summarizes the mechanical properties of HSHDC at various length scales to facilitate further development of this material and explore its potential for use in enhancing structural impact and blast resistance.

Keywords High strength-high ductility concrete • Impact resistance • High performance concrete • Micromechanics • Rate effects

15.1 Introduction

Impact and blast resistance of a material, particularly concrete for protective structures, requires high rate energy absorption, which cannot be met only by increasing the material's compressive strength. Despite this known fact, there had been a race to achieve the strongest concrete, at least until 1980s, as it offered a clear economic incentive of making lightweight structures due to the high strength-to-weight ratio of the high/ultra-high strength concretes. In the last two decades, the focus has shifted away from high strength to high performance and tensile ductility in cement-based materials. This led to the creation of ultra-ductile concretes such as Engineered Cementitious Composites (ECC) [1]. ECC can absorb large amount of energy per unit volume; however, it does not possess similar strength-to-weight ratio as ultra-high strength concretes (UHSC). The ultra-high performance concretes (UHPC) [2], extension of UHSC with the addition of fibers and microstructure improvements, do offer a good strength-to-weight ratio but their energy absorption is limited due to tension-softening behavior. This motivated the development of High Strength-High Ductility Concrete (HSHDC), which offer the performance advantages of both ECC (tensile ductility) and UHPC (compressive strength).

HSHDC, as the name suggests, combines ultra-high compressive strength (>150 MPa) and tensile ductility (>3 %) in one material [3]. The microstructure of HSHDC is tailored specifically to meet these target composite properties. The mix design of HSHDC is given in Table 15.1, and the properties of the ultra-high molecular weight polyethylene (PE) fiber used in HSHDC are given in Table 15.2. In this paper, the multi-scale mechanical characterization and investigation of HSHDC from micro-scale to composite scale to structural element scale is reviewed. At the structural scale, thin slabs of HSHDC are evaluated under drop-weight impact and are compared with similar-sized fiber-reinforced UHPC (FR-UHPC) slabs.

R. Ranade (✉)
State University of New York at Buffalo, 135 Ketter Hall, Buffalo, NY 14260, USA
e-mail: ranade@buffalo.edu

W.F. Heard • B.A. Williams
Engineer Research and Development Center (ERDC) of the US Army Corps of Engineers,
3909 Halls Ferry Rd, Vicksburg, MS 39180, USA

B. Song et al. (eds.), *Dynamic Behavior of Materials, Volume 1*,
Conference Proceedings of the Society for Experimental Mechanics Series, DOI 10.1007/978-3-319-22452-7_15

Table 15.1 Mix proportions of HSHDC

Constituent	Particle size range, μm (1 μm = 3.9 × 10^{-5} in.)	Mix proportions (by weight)	Weight per unit volume	
			(kg/m^3)	(lb/yd^3)
Cement (Class H)	30–80	1	907	1528
Microsilica (Silica Fume)	0.1–1	0.389	353	595
Ground Silica (Silica Flour)	5–100	0.277	251	423
Silica Sand	100–600	0.700	635	1070
Tap Water	–	0.208 w/cm = 0.15	189	318
HRWRA	–	0.018	16	27
PE Fiber[a]	–	0.0214	19	33

[a]Properties of the PE fiber are given in Table 15.2

Table 15.2 Geometry and mechanical/physical properties of the PE Fiber

Diameter	Length	Volume fraction	Tensile strength	Young modulus	Elongation at break	Specific gravity	Melting temp.
28 mm	12.7	2 %	3000 MPa	100 GPa	3.1 %	0.97	150 °C

15.2 Micromechanics-Based Design of HSHDC

Unlike the design of most other cementitious materials which is typically based on empirical results, the design of HSHDC is grounded in the principles of fracture mechanics at the micro-scale (micromechanics). The micromechanics-based design (originally developed for designing ECC) relies primarily on investigating and favorably tailoring the interactions between these phases (particularly fiber/matrix interactions) for achieving desirable composite tensile properties. The excellent compressive properties of HSHDC are achieved by adopting the long-standing design principles of UHPC which include reducing matrix porosity, dense particle packing, promoting mix homogeneity, using sound quality aggregates, and microstructure enhancements through heat curing. Such systematic design of HSHDC facilitates the achievement of the unique combination of compressive strength and tensile ductility.

The major steps involved in the micromechanics-based design procedure for tailoring the tensile properties of HSHDC are shown in Fig. 15.1 below. This procedure typically starts with a matrix optimized for compressed strength, along with certain types of high performance fibers (shortlisted based on strength, modulus, water/cement ratio of the matrix, etc.). The goal of this design procedure is to select the fiber type and geometry which can optimally work with matrix; although, slight matrix modifications are expected to accommodate the fiber.

Starting with the single fiber pullout tests, the fiber/matrix interaction parameters are determined. These parameters are fed into a statistical scale-linking model [4], along with an assumed fiber geometry (diameter and length), to determine the collective bridging stress (σ) of the fibers as a function of the crack opening (δ), known as the σ-δ relation. This σ-δ relation acts as a constitutive law of crack bridging for this particular fiber/matrix system, and is used to infer the maximum complementary energy of fiber bridging (J_b') and the fiber bridging stress capacity (σ_{ult}). The fiber geometry is optimized to maximize J_b' and σ_{ult}. J_b' and σ_{ult} are maximized because the micromechanics principles require (1) σ_{ult} to be greater than the matrix cracking strength (σ_{fc}), and (2) J_b' to be greater than the crack tip toughness J_{tip} to ensure multiple cracking and tensile ductility of HSHDC. Greater ratios σ_{ult}/σ_{fc} and J_b'/J_{tip} lead to greater tensile ductility and robustness of multiple cracking [5].

In case, any of the two necessary micromechanics-based conditions [(1) or (2) above] is violated, the matrix modifications such as lowering the matrix fracture toughness or introducing artificial flaws are investigated, and/or the fiber/matrix bond is altered through fiber coatings or treatments. Even when both the conditions for multiple cracking are satisfied, the design of HSHDC may be limited by the commercial availability of the optimized fiber geometry or the processability of the fibers (e.g. the high aspect ratio of the fibers may make them harder to mix homogenously, particularly in low water/cement ratio matrices such as the HSHDC matrix). The processability and fiber dispersion is improved by controlling the matrix viscosity. If none of the above corrections are successful, the same process is repeated with the next fiber until the most suitable fiber is found for that particular matrix. Composite-scale experiments are performed to verify the tensile and compressive properties of HSHDC.

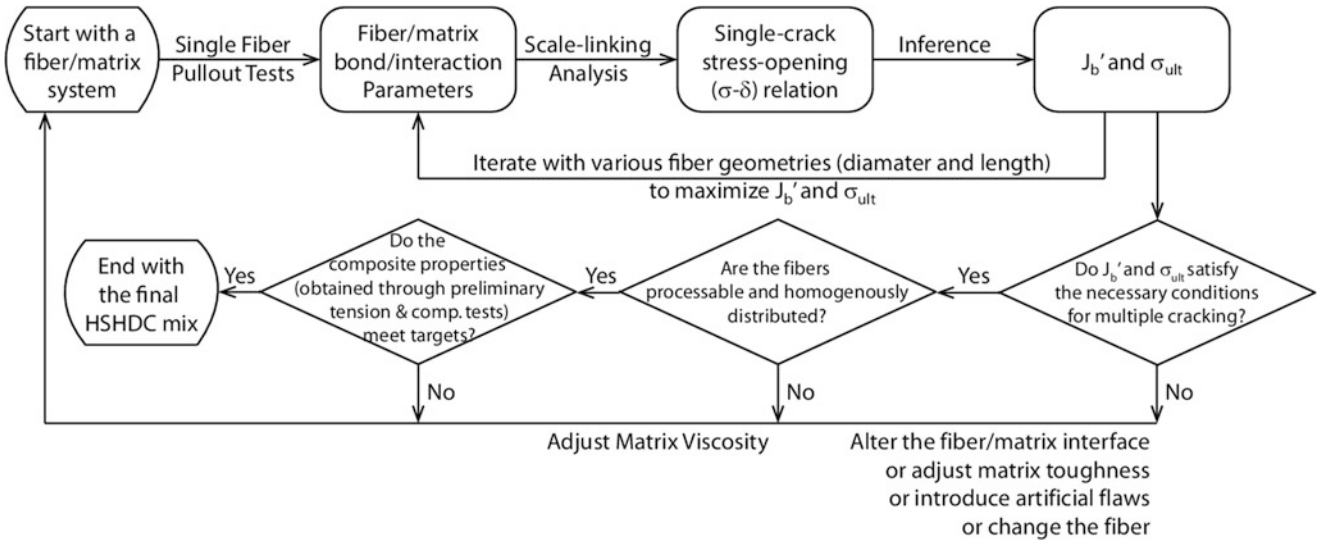

Fig. 15.1 Micromechanics-based procedure for designing HSHDC

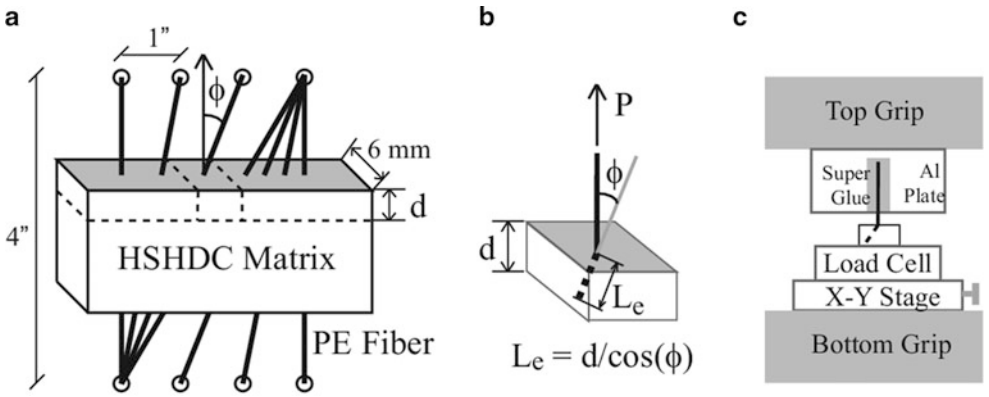

Fig. 15.2 Single-fiber pullout (SFP) test (**a**) specimen preparation for polymer fibers (**b**) individual polymer fiber SFP specimen (**c**) experimental setup

The micromechanical investigation of HSHDC is reported in Ranade et al. [6]. The average fiber/matrix interaction parameters of HSHDC obtained from several single fiber pullout tests (Fig. 15.2). The PE fiber forms high interfacial frictional bond (τ_0) of about 1.52 MPa facilitated by dense particle packing of the very high strength matrix. This high τ_0 accompanied by a negligible chemical bond (G_d), results in a high complementary energy (J_b') favorable for macroscopic strain-hardening response of HSHDC under direct tension. For comparison, the measured τ_0 for the same fiber in a moderate strength matrix has been reported to be 0.54–0.76 MPa [7]. Other fiber/matrix interaction properties of HSHDC determined in this research are snubbing coefficient ($f = 0.59$) and slip hardening parameter ($\beta = 0.003$). All micromechanical properties show wide scatter due to material inhomogeneity (similar to SHCC) at micro-length scale.

A new inclination-dependent hardening mechanism of fiber pullout in HSHDC is also discovered in Ranade el al [6], as the existing fiber/matrix interaction mechanisms [8] developed for similar strain-hardening concretes (such as ECC) are insufficient in completely describing the experimentally observed inclined fiber pullout behavior of PE fibers embedded in a very high strength HSHDC matrix. The SHCC micromechanical model in the pullout phase is modified to incorporate this mechanism. The SEM micrographs (Fig. 15.3) provide evidence for this mechanism and its mathematical formulation. The newly defined inclination hardening parameter, μ (constant property of the composite), is 386 N/(m-rad) for HSHDC.

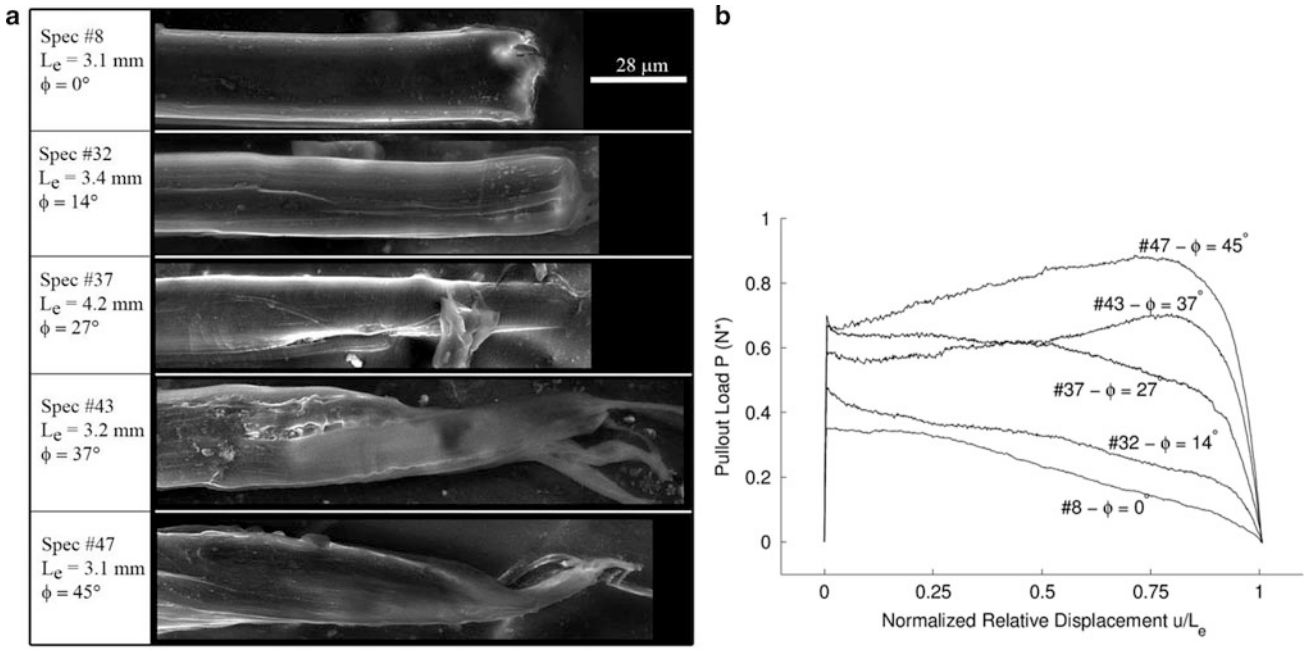

Fig. 15.3 (**a**) SEM micrographs showing increasing fibrillation of highly inclined fibers supporting the presence of inclination hardening in HSHDC observed in (**b**) Single fiber pullout curves of PE fibers embedded in HSHDC matrix

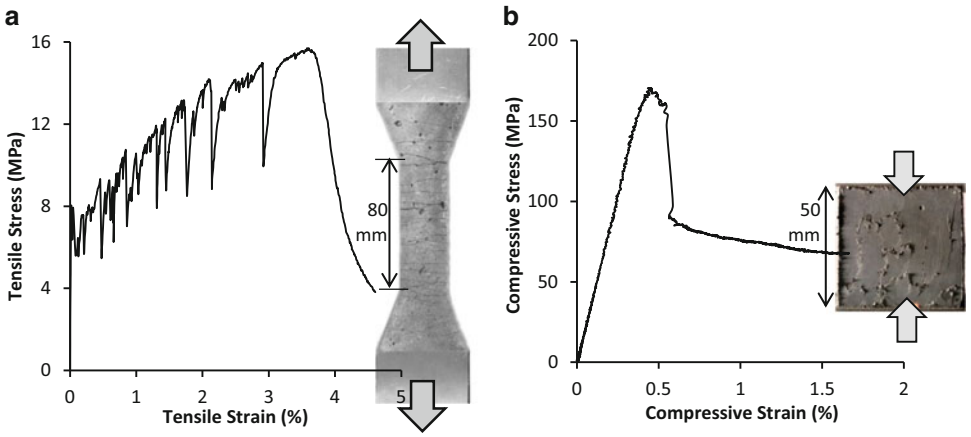

Fig. 15.4 Composite behavior of HSHDC under (**a**) direct uniaxial tension (**b**) direct uniaxial compression

15.3 Composite Properties of HSHDC

The composite-scale characterization of HSHDC is reported in Ranade et al. [3]. The behavior of HSHDC under direct uniaxial tension is shown in Fig. 15.4a. The average tensile stress capacity of HSHDC is about 14.5 MPa and average tensile strain capacity is 3.5 %. As the load increases from zero, the tensile stress inside the composite increases linear-elastically. The matrix cracks for the first time when the stress intensity factor exceeds the fracture toughness of the matrix, typically at the largest internal flaw. The crack propagates almost instantaneously throughout the section under steady-state (a direct result of micro-mechanical tailoring [9]) causing sudden drop in tensile stress as the load transfer capacity of the matrix at the section is lost. However, the fiber bridging capacity is not exceeded at the matrix cracking stress (another result of micromechanics-based design), and the tensile stress is gradually regained exceeding the first crack stress. The tensile stress increases until another crack is triggered at the next largest flaw and the process repeats until the fiber bridging capacity is exceeded by the applied tensile stress at one of these cracked sections. After this point, the tensile stress reduces

monotonically following the bridging stress-crack opening relation. Thus, the micromechanics-based design of HSHDC facilitates multiple micro-cracking of the matrix under tension which is the fundamental reason behind the extraordinary tensile ductility and specific energy of the composite.

The behavior of HSHDC under uniaxial compression is shown in Fig. 15.4b. The pre-peak branch of these curves is extremely linear and elastic, which is typical of VHSC/UHPCs. Near the peak (within about 20 % of the peak load), the stress-strain curve of HSHDC becomes non-linear and inelastic due to the nucleation of microcracks at grain boundaries, micro-defects, and other micro-scale heterogeneities. These cracks are stabilized through fiber-bridging in HSHDC resulting in a more ductile response and a flattened peak (in HSHDC) instead of a sharp peak typically observed in VHSC/UHPCs [2, 10]. Furthermore, it can be seen in Fig. 15.4b that the post-peak stress after the axial splitting of an HSHDC cube does not suddenly drop to near zero but to a residual stress value of 60–80 MPa. Thereafter, the stress gradually decreases to zero with increasing compressive displacement. Overall, HSHDC shows linear elastic behavior under uniaxial compression until 80 % of its peak strength, followed by a relatively ductile near-peak and post-peak response.

The flexural behavior of HSHDC under four-point bending (using 100 × 100 × 300 mm beams) is investigated in Ranade et al. [3]. The average modulus of rupture (MOR) of HSHDC beams is about 32 MPa and the average mid-point net deflection of the beam at MOR is about 2.5 % of the span length. The high flexural strength and ductility of HSHDC are direct results of its high compressive strength and tensile ductility. For instance, the MOR of HSHDC beams can be predicted from its properties under uniaxial tension and compression using the analytical model developed by Maalej and Li [11]. The average MOR/σ_{tc} ratio of HSHDC is 3.8, which agrees well with the analytical prediction.

15.4 Tensile Rate Effects in HSHDC

The properties of HSHDC, similar to other cement-based materials [12], are influenced by the strain/load rate [13]. As the strain rate is increased from 0.0001/s to 10/s, average first crack strength (σ_{fc}) and average ultimate tensile strength (σ_{ult}) of HSHDC dogbone specimens increase by about 53 % and 42 %, respectively, as observed in Fig. 15.5a. In spite of a relatively constant ratio of σ_{ult}/σ_{fc} with strain rate, the tensile strain capacity decreases to 2.9 % at 0.1/s and plateaus after that. Such variation in tensile strain capacity is attributable to a similar trend in average crack width which reduces from 160 μm at 0.0001/s to 120 μm at 0.1/s and plateaus for higher strain rates.

These tensile rate effects at the composite scale are caused due to the rate effects at the micro-scale, reported in Ranade et al. [13]. Almost all the fiber/matrix interaction properties, fiber properties, and matrix fracture toughness exhibit changes with displacement rate (equivalent to the strain rate in composite testing) to varying degrees. The interfacial frictional bond (τ_0) increases only slightly (by 14 %) over the six orders of displacement rates investigated in this study (0.009–900 mm/s). The absence of chemical bond between the PE fiber and HSHDC matrix makes the overall fiber/matrix bond relatively

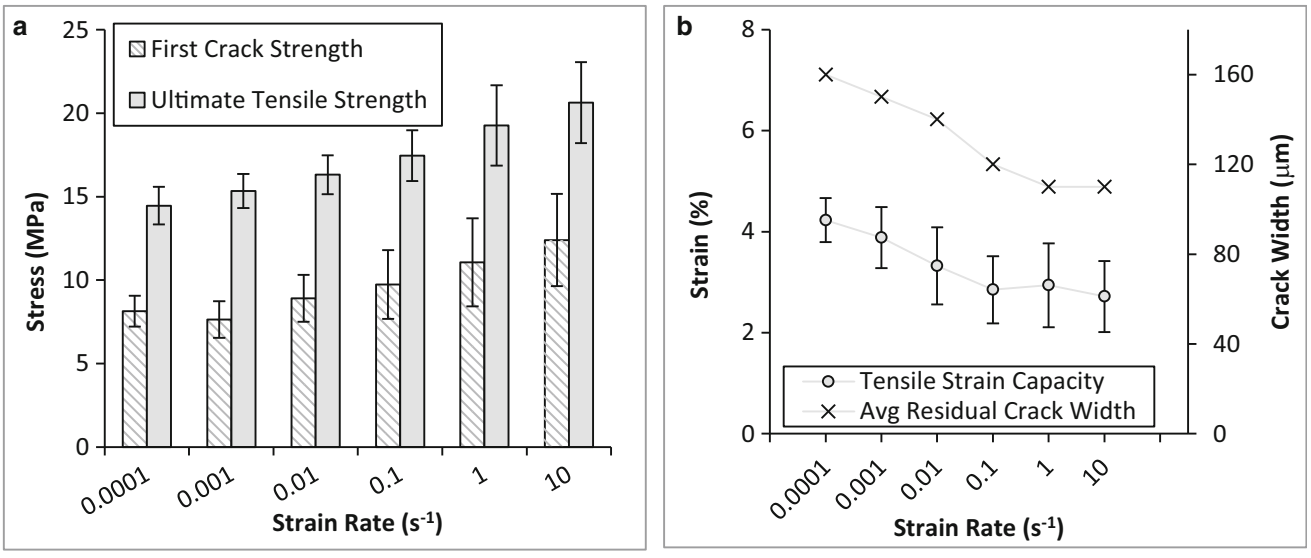

Fig. 15.5 Composite scale rate effects in HSHDC. (**a**) First crack strength and Ultimate tensile strength (**b**) Tensile strain capacity and average residual crack width

insensitive to rate effects. The changes that are the most consequential for fiber-bridging in HSHDC are the increases in PE fiber strength and modulus with displacement rate. At the fastest rate, the PE fiber strength and modulus increase by about 21 and 85 % of their respective quasi-static values. However, these increase in fiber strength and modulus, along with the increase in fiber/matrix interaction properties, result in the reduction of complementary energy (J_b') of fiber-bridging. Nevertheless, J_b' remains significantly greater (about six times) than the crack tip toughness even at the highest strain rate investigated in this study, which coupled with constant σ_{ult}/σ_{fc} ratio (due to comparable increases in matrix fracture toughness and fiber-bridging capacity) facilitates multiple cracking and energy absorbing capacity of HSHDC at all strain rates investigated in this study.

15.5 Impact Resistance of HSHDC

The behavior of thin slabs of HSHDC under multiple, moderate-velocity impacts is investigated utilizing preliminary drop-weight impact experiments (Fig. 15.6) [14]. The behavior of HSHDC slabs (300 × 300 × 25 mm) is compared with the behavior of same-sized slabs made of a fiber-reinforced Ultra-high Performance Concrete (FR-UHPC) with compressive strength greater than 200 MPa. A constant weight of 16.04 kg was dropped repeatedly on both HSHDC and FR-UHPC slabs using a cylindrical steel impact head of diameter 75 mm from a height of 1.40 m. The impacts are repeated for either 20 times or until slab failure, whichever occurs first. Almost zero rebound of the impact head either due to flexural failure of the slab or due to head penetration in the slab is deemed as 'slab failure'.

The performance of HSHDC slabs (solid curves) under repeated impacts is compared with that of the FR-UHPC slabs (dashed curves) in Fig. 15.7. Each impact produces significant inelastic tensile strains, which accumulate with increasing number of impacts. As soon as the deflection-hardening capacity of the FR-UHPC slab is exceeded, it starts to lose its impact load bearing capacity as observed by the drops in the peak contact force (PCF) in Fig. 15.7a. The drop in PCF of FR-UHPC slabs occurs rapidly after seventh to eighth impacts. In contrast, PCF in HSHDC slabs remains almost constant for all the impacts. While the FR-UHPC slabs fail under flexure before 20 impacts, HSHDC slabs maintain their integrity and continue to rebound the drop-weight assembly during all the 20 impacts. The damage tolerance of HSHDC, which is significantly higher than FR-UHPC under tension, allows the HSHDC slabs to absorb more impact energy, while maintaining their structural integrity, compared to the FR-UHPC slabs.

15.6 Modelling HSHDC in LS-Dyna

In order to investigate the structural applications of HSHDC for impact and blast resistance, the MAT_072R3 material model in the LS-Dyna library is employed. Although the MAT_072R3 model (also known as K&C model) was originally developed by Malvar et al. [15] for concrete and tension-softening FRCs, it can be adopted for HSHDC (and similar strain-hardening concretes) because it has (1) three separate fixed 'loading surfaces' (yield, ultimate, and residual), and (2) independent parameters for controlling the damage evolutions in tension and in compression. While the mathematical details of the MAT_072R3 model are presented in Malvar et al. [15] and other texts on concrete plasticity, the main features and

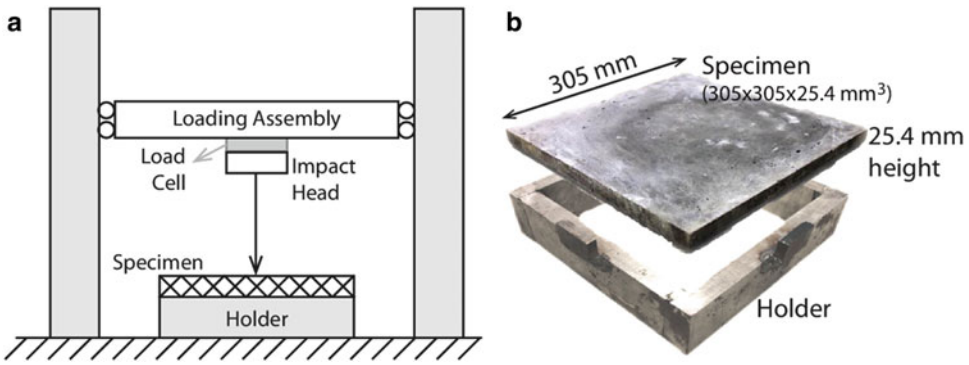

Fig. 15.6 Drop-weight impact experiment (**a**) Test setup (**b**) Specimen dimensions

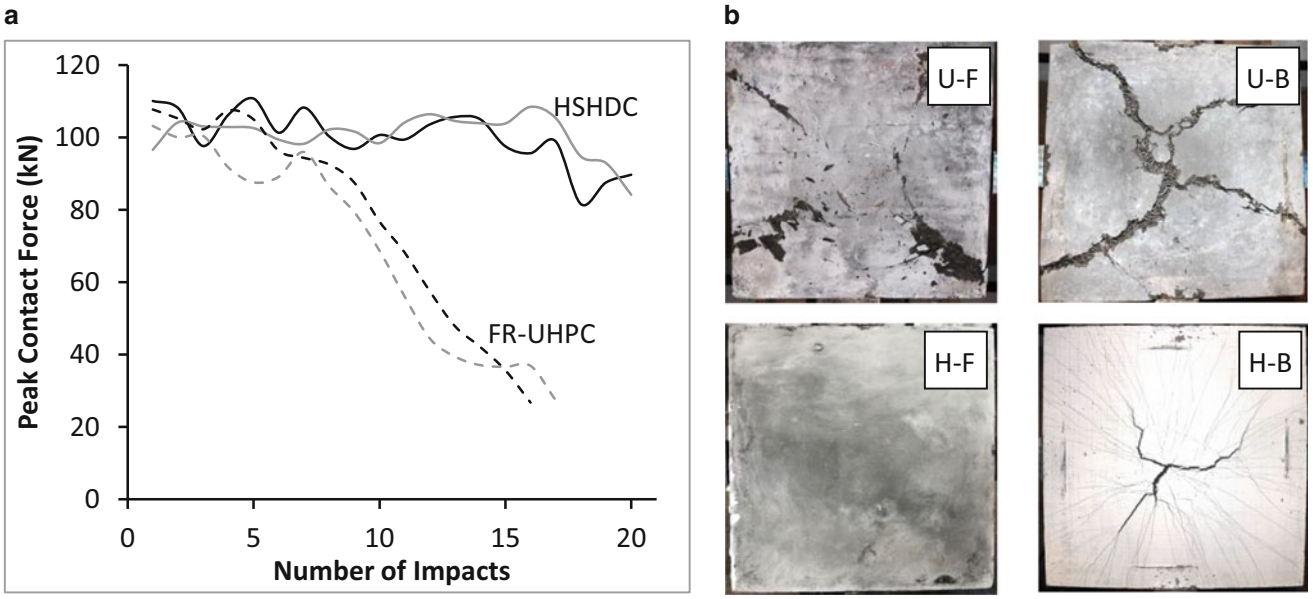

Fig. 15.7 Comparison of HSHDC and FR-UHPC slabs under multiple impacts (**a**) Peak contact force (**b**) Visual damage in the slabs of both materials*. *U is FR-UHPC and H is HSHDC; F denotes front (compression) face and B denotes back (tensile) face

Table 15.3 MAT_072R3 loading surface parameters for modelling HSHDC

a_{0y} (MPa)	a_{1y}	a_{2y} (MPa^{-1})	a_0	a_1	a_2	a_{1f}	a_{2f}
22.6×10^6	0.397	1.2×10^{-9}	24×10^6	0.366	4.91×10^{-10}	0.356	4.80×10^{-10}

setup of this model with all the inputs required for simulating HSHDC using the MAT_072R3 model are given in Ranade et al. [15].

The input parameters for the MAT_072R3 material model in LS-Dyna can be broadly classified into three categories: (1) loading surfaces, (2) damage accumulation, and (3) other inputs [15]. The eight parameters of MAT_072R3 grouped as: (a_{0y}, a_{1y}, a_{2y}), (a_0, a_1, a_2), and (a_{1f}, a_{2f}) describe the $p - \Delta\sigma$ loading curves on the compressive meridian of yield, maximum, and residual loading surfaces, respectively. As noted in Malvar et al. [15], the 3D failure surface in the post-elastic stage moves between three fixed 'loading surfaces', namely yield, maximum, and residual. Mathematically, at a particular damage state represented by damage parameter η in MAT_072R3, the failure surface is a linear combination of either the yield and the maximum or the maximum and the residual loading surfaces with coefficients η and $(1 - \eta)$. A combination of uniaxial test results conducted by the authors and previous multi-axial tests on concretes with similar compressive strength are used as known data points (p, $\Delta\sigma$) to determine the eight parameters for modelling HSHDC, noted in Table 15.3.

The damage parameter η is defined as a function of cumulative effective plastic strain parameter, λ in MAT_072R3. The parameter λ above is computed from the tensorial plastic strains, ε_{ij}^{p}, in the MAT_072R3 [15]. The η-λ damage function is input by the user (Table 15.4) based on the shape of the material's experimental uniaxial compressive behaviour. The values of the damage scaling parameters b_1 and b_2 used for the SHCC in this study are determined by matching the computed stress-strain responses of a single element with the experimental curves, and are set equal to -0.55 and -20, respectively.

Other parameters required as inputs in the MAT_072R3 model are density (2400 kg/m^3), Poisson ratio (0.20), and localization width of the crack (LOCWIDTH = 2 mm). LOCWIDTH is assumed equal to the element size, which is 2 mm, to prevent localization instabilities and spurious mesh sensitivity. Decreasing LOCWIDTH increases the observed ductility in both tension and compression.

All the model parameters discussed thus far for defining the failure surface capture only the *deviatoric* behavior of the material, and therefore, an 'equation of state' (EOS), which defines the *hydrostatic* behavior of a material by relating the hydrostatic pressure to the volumetric strain, is needed to completely describe the material behavior [15]. For this purpose, the EOS of type 8 (EOS 8) in LS-Dyna, which inputs tabulated pressure-volumetric strain data points (linear variation is assumed between the specified points) along with instantaneous bulk modulus at these points (for unloading), is used. The

Table 15.4 MAT_072R3 damage function $\eta-\lambda$ for modelling HSHDC

λ	0	1.2×10^{-5}	2.4×10^{-5}	4×10^{-5}	5.6×10^{-5}	7.2×10^{-5}	8.8×10^{-5}	1.0×10^{-4}	2.5×10^{-4}	7.0×10^{-4}	2.5×10^{-3}	10	1.0×10^{10}
η	0	0.85	0.97	0.99	1	0.99	0.88	0.3	0.2	0.1	0	0	0

rate effect on the material strength is incorporated in the model by specifying a 'load curve' in LS-Dyna, by relating dynamic increase factors (DIF) to strain rate. Failure of the material is defined using tensile and compressive erosion criteria in this study. The erosion criterion (using MAT_ADD_EROSION keyword in LS-Dyna) for tensile strain is set at 2.9 %, and that for hydrostatic pressure is set at 400 MPa. Using all the above parameters, the observed uniaxial stress-strain curves of HSHDC are satisfactorily modeled at various strain rates. Furthermore, the impact performance of HSHDC slabs (discussed above) is also satisfactorily modeled using this material model; for details, the reader is referred to Ranade [14].

15.7 Conclusions and Future Research and Applications

The development of HSHDC has opened a new avenue for material research and development, which, instead of trading-off strength for ductility/durability (and vice-versa), achieves both the objectives simultaneously. The tensile rate effects investigation reveals that the material remains ductile at high rates, which, is promising for high energy applications such as impacts and blasts; however, the strain rates are a lot higher in such events and the material is yet to be tested at these rates. Furthermore, the behavior of HSHDC with conventional steel reinforcement must be quantified in the future, as most potential structural applications of HSHDC will contain such reinforcement. In addition to structural resilience, HSHDC is also expected to be an extremely durable material owing to its tight crack width and tensile ductility. Integrated life cycle assessments investigating both the resilience and sustainability of a structure together are expected to further reveal the potential uses of HSHDC in civil and military infrastructure.

Acknowledgments The authors would like to thank Lafarge, Holcim, WR Grace, US Silica, and Honeywell for providing the materials for this research. Permission to publish was granted by the Director, Geotechnical and Structures Laboratory at ERDC.

References

1. Li, V.C.: On engineered cementitious composites (ECC)—a review of the material and its applications. J. Adv. Concr. Technol. **1**(3), 215–230 (2003)
2. Russell, H.G., Graybeal, B.A.: Ultra-high performance concrete: a state-of-the-art report for the Bridge Community, Publication No. FHWA-HRT-13-060, pp. 1–25. US DoT, Federeal Highway Administration, McLean, VA (2013)
3. Ranade, R., Li, V.C., Stults, M.D., Heard, W.F., Rushing, T.S.: Composite mechanical properties of high strength-high ductility concrete. ACI Mater. J. **110**(4), 413–422 (2013)
4. Li, V.C., Wang, Y., Backer, S.: A micromechanical model of tension-softening and bridging toughening of short random fiber reinforced brittle matrix composites. J. Mech. Phys. Solids **39**(5), 607–625 (1991)
5. Kanda, T., Li, V.C.: Multiple cracking sequence and saturation in fiber reinforced cementitious composites. Concr. Res. Technol. **9**(2), 19–33 (1998)
6. Ranade, R., Li, V.C., Stults, M.D., Rushing, T.S., Roth, J., Heard, W.F.: Micromechanics of high strength-high ductility concrete. ACI Mater. J. **110**(4), 375–384 (2013)
7. Li, V.C., Maalej, M.: Effect of plasma treatment of polyethylene fibers on interface and cementitious composite properties. J. Am. Ceram. Soc. **79**(1), 74–78 (1996)
8. Lin, Z., Kanda, T., Li, V.C.: On interface property characterization and performance of fiber reinforced cementitious composites. J. Concr. Sci. Eng. **1**, 173–184 (1999)
9. Li, V.C., Wang, S., Wu, C.: Tensile strain-hardening behavior of PVA-ECC. ACI Mater. J. **98**(6), 483–492 (2001)
10. Wight, J.K., MacGregor, J.G.: Stress-strain Curves for Concrete. In: Wight, J.K., MacGregor, J.G. (eds.) Reinforced Concrete: Mechanics and Design, 5th ed, pp. 64–70. Upper Saddle River, NJ: Prentice Hall (2009)
11. Maalej, M., Li, V.C.: Flexural/tensile-strength ratio in engineered cementitious composites. J. Mater. Civ. Eng. **6**(4), 513–528 (1994)
12. Bischoff, P.H., Perry, S.H.: Compressive behavior of concrete at high strain rates. J. Mater. Struct. **24**, 425–450 (1991)
13. Ranade, R., Li, V.C., Heard, W.F.: Tensile rate effects in high strength-high ductility concrete. Cem. Concr. Res. **68**, 94–104 (2014)
14. Ranade, R.: Advanced cementitious composites development for resilient and sustainable infrastructure, pp. 216–297. Ph.D. Dissertation, University of Michigan (2014)
15. Malvar, L.J., Crawford, J.E., Wesevich, J.W., Simons, D.: A plasticity concrete material model for DYNA3D. Int. J. Impact Eng. **19**(9–10), 847–873 (1997)
16. Ranade, R., Li, V.C.: Material model for SIMULATING SHCC in LS-Dyna. In: Proceedings of RILEM SHCC-3, pp. 235–242, Dordrecht, Netherlands, 3–5 Nov 2014